ACS EARTH AND SPACE CHEMISTRY

http://pubs.acs.org/journal/aesccq

Article

Molecular Dynamics Simulations of Electrical Conductivity of NaCl Solutions at High Temperatures and Pressures

Rajorshi Chattopadhyay* and Sandro Jahn

Cite This: *ACS Earth Space Chem.* 2025, 9, 2313−2323

Read Online

ACCESS | Metrics & More | Article Recommendations | Supporting Information

ABSTRACT: Electrical conductivity measurements of subsurface geochemical systems are used to detect the presence of aqueous fluids that drive chemical reactions in the Earth's crust and mantle. Experiments on NaCl solutions show that their electrical conductivities (σ) have a non-monotonic dependence on pressure and temperature. In this paper, we study this important property based on an atomic-scale simulation approach. We perform molecular dynamics (MD) simulations of 1.05 mol/kg NaCl solutions along 473 K, 673 and 1073 K isotherms at pressures from 0.1 to 5 GPa. Two different interaction models are used for our MD simulations: ReaxFF, a many-body dissociative force field, and SPC/E, a two-body rigid force field. The simulations suggest that the non-monotonic behavior of the electrical conductivity is caused by a complex interplay between ion self-diffusion and ion pairing. Both models differ in their predictions. Electrical conductivity in the ReaxFF simulations is influenced by both ion self-diffusion and ion pairing at all the studied conditions, whereas the conductivity from the SPC/E model is completely diffusion-driven at low temperatures, with ion pairing effects observed at higher temperatures. We find that the absolute values of σ obtained from MD simulations are largely consistent with the experimental data up to about 1 GPa, but the surprisingly large increase of σ with temperature at higher pressures reported recently could not be reproduced.

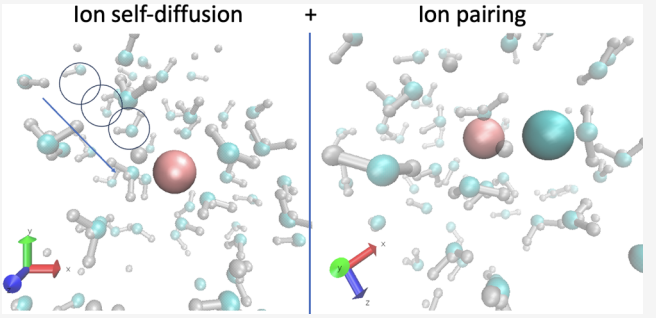

KEYWORDS: *molecular dynamics simulations, aqueous fluids, supercritical conditions, electrical conductivity, self-diffusion, classical potentials, reactive force fields*

1. INTRODUCTION

Aqueous fluids play an important role in characterizing the thermophysical properties of many subsurface geochemical systems. Regions of anomalously high electrical conductivity have been reported in the lower crust as well as in arc and subduction zone settings.[1−4] Several reasons have been suggested to explain the occurrence of these zones, including but not limited to changes in the mineralogy,[5,6] partial melts[7,8] and saline fluids.[9−12] However, in most of these zones a combination of different contributions is present with aqueous fluids playing a dominant role, especially in subduction zones.[2,6] While pure water has a relatively low electrical conductivity,[13,14] dissolved salts enhance the conductivity of these fluids. Fluid inclusion studies from subduction zones suggest that NaCl is the dominant solute under conditions of the lower crust and upper mantle.[15] Several magnetotelluric surveys[16,17] have been conducted to understand the nature of aqueous fluids in high temperature and high pressure geologic environments. However, interpretation of these data is difficult due to the lack of electrical conductivity data for such fluids, especially at pressures above 1 GPa.

The electrical conductivity of NaCl solutions is a complex function of temperature, pressure and concentration. Over the years, the determination of electrical conductivity of NaCl solutions at supercritical conditions has been the aim of several experimental studies.[18−23] Measurements of electrical conductivity along isobars ranging from 0.025 to 1 GPa show an initial increase up to about 400 °C followed by a decrease.[18−21] When measured along isotherms, conductivity increases rapidly with increase in pressure at low fluid densities (<0.5−0.6 g/cm^3).[19,22,23] The rate of increase gradually reduces with density[22,23] and eventually a decrease in conductivity is observed starting at a fluid density of about 0.8 g/cm^3.[19] The density at which this conductivity maximum is observed depends on the concentration of the NaCl solution.[19,20] Quist and Marshall[19] qualitatively explained this behavior using density and ion pairing effects[19] whereas Lee et al.[24] attributed it to residence times of water molecules in the hydration shells of supercritical fluids. In fact, the influence of

Received: May 19, 2025
Revised: July 28, 2025
Accepted: August 5, 2025
Published: September 3, 2025

ion association is expected to be particularly dominant at high temperatures due to the low dielectric constant of water.[21] Such high-temperature and high-pressure experiments are not straightforward because of technical challenges as well as difficult preparation procedures. Guo and Keppler[25] extended the temperature and pressure ranges to 900 °C and 5 GPa, respectively, and observed a strong increase in the electrical conductivity of NaCl solutions with temperature, particularly along 3 to 5 GPa isobars. This observation is in contrast to the temperature dependence observed in other experimental data sets at pressures up to 1 GPa,[19,21] where the electrical conductivity shows a rather weak temperature dependence. Conductivity measurements of aqueous KCl solutions up to 5 GPa[26] yielded a similarly weak temperature dependence along the 3 to 5 GPa isobars. Given the similar chemical and physical properties of K and Na, the observed difference in the qualitative temperature dependence of their electrical conductivities is unexpected and warrants further investigation.

Molecular dynamics (MD) simulations support the interpretation of experimental observations by explicit modeling of the motions of ions and water molecules, which provides insight into the mechanisms of electrical conduction at the nanoscale. Classical molecular dynamics (CMD) simulations with pairwise interaction potentials have been successfully used to study several properties of electrolytes under conditions difficult to achieve in the laboratory. For example, previous simulation studies have addressed the self-diffusion coefficients of Na^+ and Cl^- ions in a range of conditions starting from room temperature to supercritical conditions,[24,27,28] hydration shell structures of ions in supercritical water,[29] NaCl ion association in supercritical brines[30] or electrical conductivity of NaCl solutions in a wide range of conditions.[24,31−37] One of the most widely used water models, called the SPC/E model, has been very successful in reproducing the bulk properties of pure water[38] but shows a systematic underestimation of electrical conductivity at ambient conditions.[39] Pairwise interaction potentials are also limited by their inability to represent bonded interactions in the limit of dissociation, thereby failing to model reactive systems involving extensive formation and breakage of chemical bonds like the Grotthuss mechanism of proton diffusion in water.[40] This is remedied by reactive force fields such as the ReaxFF,[41] which are empirically fitted to model such reactive systems.[42−44] Recently, a new ReaxFF parameter set was developed by Fedkin et al.[45] for aqueous electrolytes. This potential successfully reproduced the structural and transport properties of electrolytes at ambient conditions.[45] However, empirical force fields come with a caveat—systematic errors may arise if these force fields are extrapolated to systems too far beyond what they have been fitted on. Therefore, MD simulations with such force fields must be adequately benchmarked to understand their extrapolation capabilities.

In this paper, we perform MD simulations using the ReaxFF and SPC/E interaction models to systematically investigate the role of the functional form of the underlying force fields in the prediction of electrical conductivity. Given the large increase in conductivity along the 3 to 5 GPa isobars[25] we explore whether different MD models can reproduce this trend and provide a mechanistic insight into its origin. Further, we examine the influence of two dominant factors governing electrical conductivity at temperatures between 200 and 800 °C and pressures between 0.1 and 5 GPa. For that, the total electrical conductivity is separated into contributions from ion self-diffusion and ion association to assess the influence of each factor in determining temperature- and pressure-induced variations. Finally, the electrical conductivities calculated from the two interaction models are discussed in terms of available experimental and simulation data and possible implications for the interpretation of geophysical measurements in fluid-containing high conductivity regions of the lower crust and upper mantle.

2. METHODS

2.1. Simulation Protocol. MD simulations of 1.05 mol/kg aqueous Na-Cl solutions are performed in 3D periodically replicated simulation boxes. The concentration is chosen to match that in the experimental study of Guo and Keppler.[25] Two different simulation boxes are prepared as shown in Table 1. Box #1 is used for simulations with the SPC/E[46] model. In order to account for higher computational expense, box #2 is used for simulations with the ReaxFF model. To prepare the boxes, first a simulation cell containing only water molecules is equilibrated at 298 K, 1 bar using the SPC/E model.[46] The solutions are prepared by replacing some of the water molecules with Na-Cl ion pairs resulting in box #1 containing 1960 water molecules, 36 Na-Cl pairs and box #2 containing 757 water molecules, 14 Na-Cl pairs. To calculate the static dielectric constant, ϵ, of the solvent, simulations are conducted with pure water using boxes #3 and #4 containing 729 and 2197 water molecules, respectively. The interaction parameters for calculating pairwise van der Waals interactions, short-range interactions and Coulomb interactions in the SPC/E model are listed in Table S1. Reactive MD simulations of aqueous NaCl solutions as well as pure water are performed using the recently developed ReaxFF parameters for aqueous electrolytes.[45] An overview of the functional forms of the two models is provided in the SI. The time step for the SPC/E simulations is 0.5 fs. Since ReaxFF is a dissociative force field and accounts for several intramolecular degrees of freedom, a shorter time step of 0.25 fs is used. The simulation boxes are equilibrated for 10^6 timesteps in the *NPT* ensemble, that is at constant pressure, P, temperature, T, and number of particles, N. Production simulations are then conducted at constant volume, V, in the *NVT* ensemble for 20 ns in case of the SPC/E model and for between 5 and 10 ns with the ReaxFF model. Nosé-Hoover thermostat and barostat are used to control the temperature and pressure at the target values. The production simulation trajectories are used to calculate electrical conductivities, self-diffusion coefficients and ion association. Additional production simulations are conducted in the *NPT* ensemble to calculate the density of NaCl solutions. All simulations are performed with the LAMMPS simulation package.[47]

Table 1. Contents of Simulation Boxes Including Solute Molality and Mass Fraction

Box no.	Contents	Molality (mol/kg)	Weight %
#1	1960 H_2O, 36 Na-Cl pairs	1.02	5.63
#2	757 H_2O, 14 Na-Cl pairs	1.02	5.63
#3	729 H_2O	-	-
#4	2197 H_2O	-	-

2.2. Electrical Conductivity and Its Decomposition. The electrical conductivity, σ, of NaCl solutions is calculated using the Green−Kubo relation:[48,49]

https://doi.org/10.1021/acsearthspacechem.5c00139
ACS Earth Space Chem. 2025, 9, 2313−2323

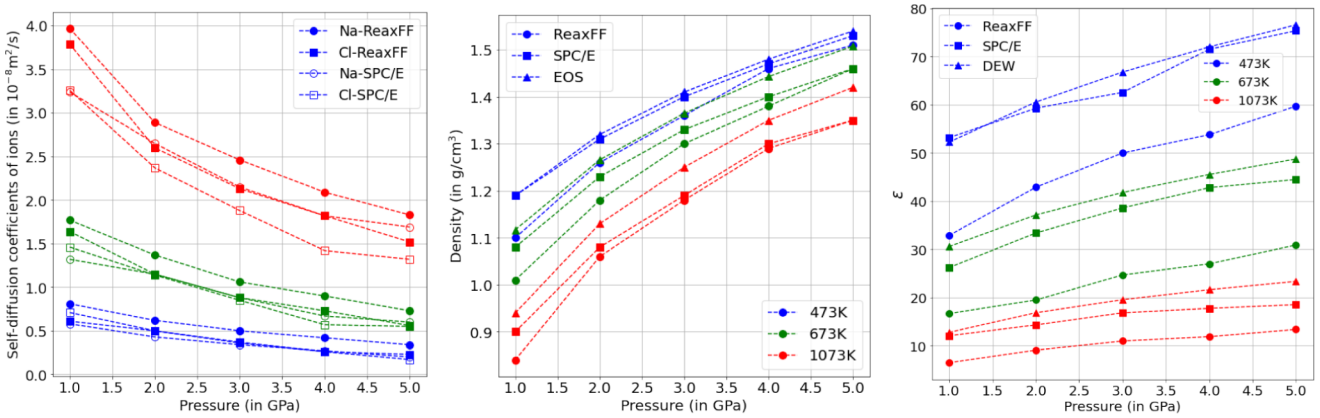

Figure 1. Left: Self-diffusion coefficients of cations and anions in 1.05 mol/kg solutions obtained from the SPC/E and ReaxFF models along isotherms. Middle: Bulk density of 1.05 mol/kg solutions obtained from SPC/E and ReaxFF models compared against EOS from Mantegazzi et al.[52] along isotherms. Right: Static dielectric constant of pure water obtained from SPC/E and ReaxFF models compared against data from the DEW model.[53]

$$\sigma = \frac{1}{3Vk_BT}\int_0^\infty \langle \vec{j}(0)\vec{j}(t)\rangle \mathrm{d}t \tag{1}$$

where

$$\vec{j}(t) = \sum_i q_i \vec{v}_i \tag{2}$$

with $\vec{j}(t)$ being the charge current at time t, k_B the Boltzmann constant, q_i the partial charge and $\vec{v}_i$ the velocity vector of ion i. The angular brackets denote ensemble average over the entire trajectory. In practice, eq 1 is integrated to a finite time t_{max}, at which the charge correlation function has decayed to zero. It has been shown that σ of NaCl solutions calculated using eq 1 does not show any finite-size effects.[39] Eq 1 is derived using the linear response theory and hence does not require an external electric field to be applied in the simulations.

The Green−Kubo integral in eq 1 can be written as a summation of contributions from individual ionic species of type I given by:

$$\sigma_I = \frac{1}{3Vk_BT}\int_0^\infty \langle \vec{j}(0)\vec{j}_I(t)\rangle \mathrm{d}t \tag{3}$$

This can be further divided into self- and cross-correlation terms[50] as

$$\sigma_I = \frac{\rho_I q_I^2 D_I}{k_BT} + \sum_L \frac{q_I q_L}{Vk_BT}\int_0^\infty C_{IL}(t)\mathrm{d}t \tag{4}$$

where ρ_I is the number density of ion type I and D_I is the self-diffusion coefficient obtained by integrating the velocity autocorrelation function of species type I.

$$D_I = \frac{1}{3N_I}\int_0^\infty \left\langle \sum_{i\epsilon I} \vec{v}_i(0)\vec{v}_i(t)\right\rangle \mathrm{d}t \tag{5}$$

where N_I is the number of species of type I. Since we approximate the self-diffusion coefficients of the ions from simulation boxes having finite size, correction terms according to the approach of Yeh and Hummer[51] are added.

C_{IL} is the velocity cross-correlation function between ions of type I and L

$$C_{IL}(t) = \frac{1}{3}\left\langle \sum_{i\epsilon I}\sum_{l\epsilon L} \vec{v}_i(0)\vec{v}_l(t)\right\rangle \tag{6}$$

When I and L are identical, the term $i = l$ is excluded. For infinitely dilute solutions, C_{IL} can be neglected and eq 4 reduces to the Nernst−Einstein relation for ionic conductivity. Eq 1 is integrated over 1 to 5 ps for SPC/E and 10 to 20 ps for ReaxFF simulations. In order to achieve convergence, the average over two successive time chunks of 400 ps for SPC/E and 2000 ps for ReaxFF are taken as the final conductivity value (Figure S1). ReaxFF requires larger time chucks and longer integration times due to the nature of the underlying autocorrelation functions. ReaxFF being a dissociative force field accounts for several intramolecular degrees of freedom, and hence more data points are required for better averaging. SPC/E, on the other hand, produces much smoother autocorrelation functions that converge to zero faster than those from ReaxFF.

2.3. Static Dielectric Constant ϵ. Under periodic boundary conditions (PBC), ϵ of isotropic fluids can be calculated as:

$$\epsilon = 1 + \frac{(\langle|\vec{M}|^2\rangle - \langle|\vec{M}|\rangle^2)}{3\epsilon_0 Vk_BT} \tag{7}$$

where

$$\vec{M} = \sum_{\text{water molecules}} \vec{\mu}_i \tag{8}$$

is the total dipole moment of all the solvent water molecules in the system. Since ReaxFF does not guarantee zero net charge on water molecules, the dipole moment was calculated with respect to the center of mass (COM) with instantaneous charges. This makes the calculated dipole moments independent of the absolute positions of the atoms.

3. RESULTS

Figure 1 (left) shows the self-diffusion coefficients D_I of Na^+ and Cl^- ions obtained from eq 5 for the two models. Numerical values of D_I are listed in Table S2, and convergence plots are shown in Figures S2 and S3. D_I of cations and anions for both models increase with increasing temperature and decrease with increasing pressure. The ReaxFF model predicts

https://doi.org/10.1021/acsearthspacechem.5c00139
ACS Earth Space Chem. 2025, 9, 2313−2323

that the cations diffuse faster than the anions at all conditions. For the SPC/E model, the anion D_I is higher at lower pressures. At high pressure, there is a temperature-dependent cross-over, after which the cations diffuse faster.

Figure 1 (middle) compares bulk densities predicted by the ReaxFF and SPC/E models against the equation of state (EOS) of Mantegazzi et al.[52] Numerical values are provided in Table S3. The density predictions from the three models follow the following order: $\rho_{ReaxFF} < \rho_{SPC/E} < \rho_{EOS}$. The underestimation of the bulk densities by ReaxFF is particularly large at low pressures (~10%) but reduces to ~1% at higher pressures. Values of ϵ calculated from the two models and the Deep Earth Water (DEW) model[53] show the following trend: $\epsilon_{ReaxFF} < \epsilon_{SPC/E} < \epsilon_{DEW}$, as shown in Figure 1 (right). Numerical values of ϵ obtained from different models are listed in Table S4 and convergence plots are shown in Figure S4.

Table 2 lists the electrical conductivity σ of 1.05 mol/kg NaCl solution calculated using the SPC/E and ReaxFF models

Table 2. σ (in S/M) of 1.05 Mol/Kg Solutions along 473 K, 673 and 1073 K Isotherms[abc]

Temperature	Pressure	σ (SPC/E)	σ (ReaxFF)
473 K	1.0 GPa	24(1)	10(1)
	2.0 GPa	20(1)	14(1)
	3.0 GPa	16(1)	15.4(7)
	4.0 GPa	12.6(6)	13.4(3)
	5.0 GPa	9.7(3)	12(2)
673 K	1.0 GPa	32(1)	10.4(7)
	2.0 GPa	28.7(7)	16(2)
	3.0 GPa	27.0(3)	15(1)
	4.0 GPa	23.8(6)	20.5(2)
	5.0 GPa	20.6(9)	16(2)
1073 K	1.0 GPa	29(3)	15.2(8)
	2.0 GPa	28(4)	17.5(5)
	3.0 GPa	32(1)	16(1)
	4.0 GPa	28(1)	18.8(5)
	5.0 GPa	25(2)	18(1)

[a]Number in the bracket is the error in the last significant digit. [b]Error is calculated from variability of data once convergence is achieved. [c]Convergence plots are shown in Figure S1.

along three isotherms. Figure 2 compares σ along different isotherms (a,b) and isobars (c,d). The electrical conductivities predicted by the ReaxFF model are always lower than those of the SPC/E model. As shown in Figure 2b, the SPC/E model predicts a monotonic decrease of σ with pressure at 473 and 673 K, in agreement with previous simulation studies.[31] At 1073 K, this monotonic trend is no longer observed, and a shallow maximum appears in σ at ~3 GPa. σ from the ReaxFF model have maxima at 3 GPa (473 K) and 4 GPa (673 K), whereas at 1073 K σ is almost constant as shown in Figure 2a.

From Figure 2(c,d) it can be inferred that both the models show an initial increase in σ with temperature (within error bars). For the SPC/E model, a prominent decrease in conductivity is observed at higher temperatures along 1 and 2 GPa isobars whereas no such systematic trends can be delineated from conductivity obtained from the ReaxFF model. This is due to the varying influence of ion self-diffusion and ion association, which is discussed in detail in the next section.

4. DISCUSSION

4.1. Influence of Ion Diffusion and Ion Association on Electrical Conductivity.

4.1.1. Pressure Dependence. Anion self-diffusion coefficients calculated with the ReaxFF potential are lower than the cation self-diffusion coefficients, in agreement with previous ReaxFF simulations of NaCl solutions at ambient conditions.[45] For the SPC/E model, a higher anion D_I at lower pressures is consistent with simulation data at ambient conditions with non-dissociative polarizable and non-polarizable interaction potentials[35] and data up to 80 °C[27] with the SPC/E model used in this study. Sakuma et al.[31] calculated D_I at high temperatures and pressures up to 2 GPa with a non-dissociative interaction potential. Their data also predict higher D_I for anions than cations for 0.6 and 1.8 m NaCl solutions at 673 and 973 K.

Ionic mobilities in aqueous solutions depend on the bulk density of the solution as well as the local hydration shell sizes of the ions. The Na-O and Cl-O pair correlation functions obtained with both the models are shown in Figures S12 and S14. Although the sizes of the hydration shells become smaller with increasing pressure (more pronounced for the anion as compared to the cation), increase in bulk density (Figure 1 (middle) leads to overall decrease in ionic mobilities with pressure, as shown in Figure 1 (left). The trends in D_I observed in Figure 1 (left) are correlated with the trends in the bulk density predicted by the two models shown in Figure 1 (middle). Lower densities predicted by ReaxFF lead to higher D_I for both cations and anions, compared to the SPC/E model. However, although the densities predicted by the two models converge at higher pressures, there is a significant difference between D_I at these conditions, particularly for cations. Hence, density differences alone cannot explain the differences in D_I. A likely reason for that is that SPC/E and ReaxFF have completely different functional forms for short-range and long-range interactions, which affects the calculated transport properties and hydration shell structures. This is seen in Figure S12 where Cl-O pair correlation functions from the ReaxFF model show a sharp peak at 3.0 Å in addition to a broader peak at 3.4−3.9 Å. This sharp peak is due to a compact shell of 4 to 5 water molecules having significantly higher residence times, as shown in Figure S13.

The decompositions of σ into contributions from the velocity autocorrelation and cross-correlation functions (eq 4) for both potentials are shown in Figure 3. The numerical values are provided in Tables S5 and S6, respectively. This separation of σ highlights the competing effects of ion self-diffusion and ion pairing. Since ion self-diffusion is a function of density, its contribution to σ also depends on density. The contributions of cross-correlation terms for like ions are close to zero for both potentials at all conditions due to short correlation times of the underlying velocity correlation functions. For the SPC/E model, the cross-correlation contribution of oppositely charged ions is also close to zero at 473 and 673 K making σ completely diffusion controlled. Since the total contribution of ion self-diffusion to σ decreases with increasing pressure (Figure S5), the SPC/E model predicts a decrease in σ with pressure at 473 and 673 K as shown in Figure 2b. At 1073 K, Figure 3 (right) shows a significantly larger negative contribution of oppositely charged ion pairs, which reduces with increasing pressure in the SPC/E simulations. The large negative contribution of ion pairing at high temperature and low pressures (1073 K, ~1−3 GPa) is due to the small ϵ of

https://doi.org/10.1021/acsearthspacechem.5c00139
ACS Earth Space Chem. 2025, 9, 2313−2323

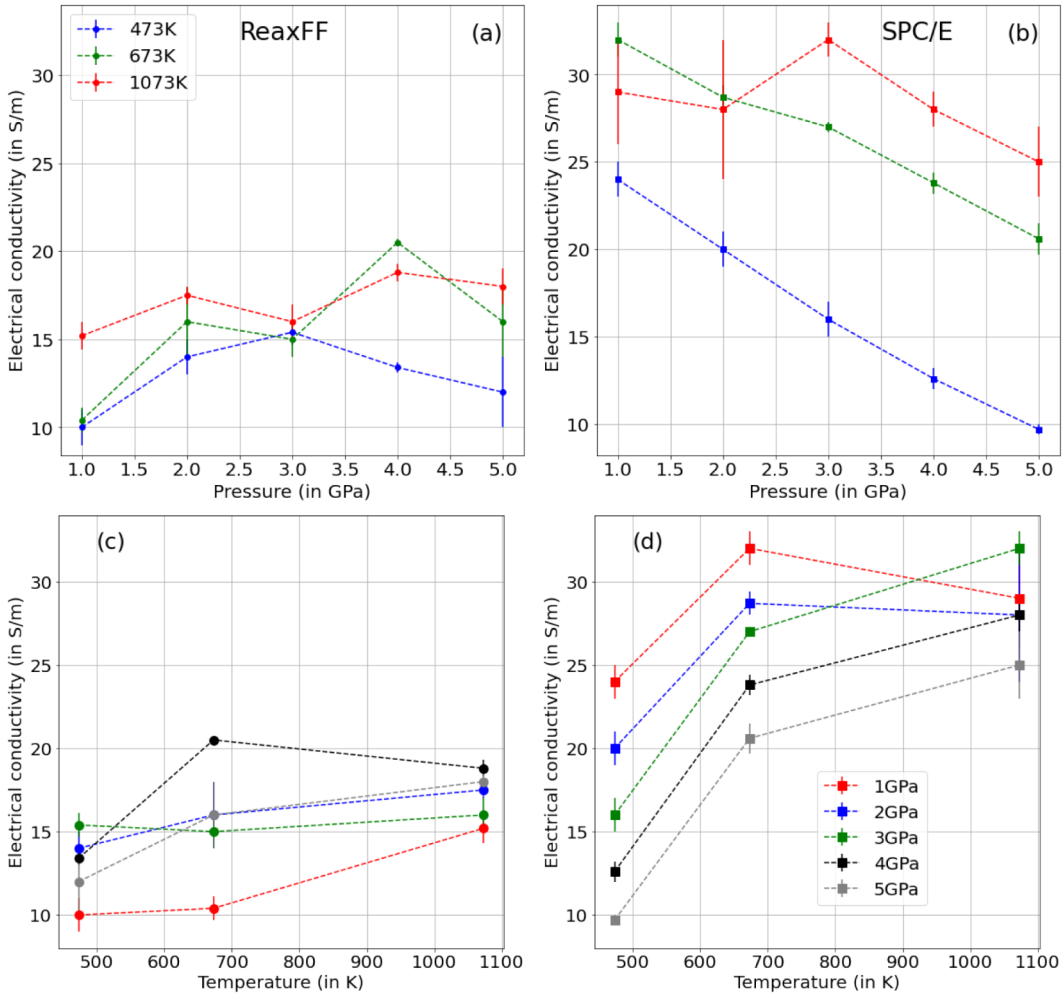

Figure 2. (a, b): σ of 1.05 mol/kg solutions obtained from the ReaxFF (a) and SPC/E (b) models along different isotherms. (c, d): σ of 1.05 mol/kg solutions obtained from the ReaxFF (c) and SPC/E (d) models along different isobars.

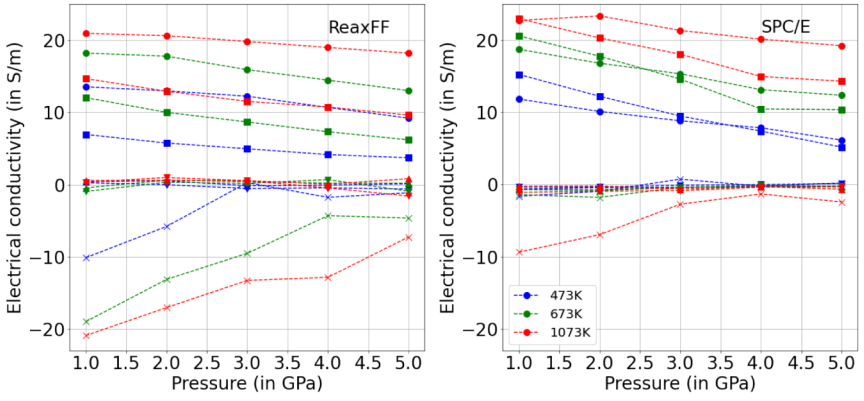

Figure 3. Decomposition of σ for 1.05 mol/kg solution from the ReaxFF model (left) and the SPC/E model (right) along different isotherms. Symbols are used to show different components of σ - dot: cation self-diffusion, square: anion self-diffusion, inverted triangle: cation cross-correlation, triangle: anion cross-correlation, cross: cation−anion cross-correlation.

water that promotes ion pair formation (and hence lower percentages of free ions as shown in Table 3) at these conditions. With increasing pressure along the 1073 K isotherm, ϵ of water increases (Figure 1 (right)) thereby increasing the ability of water to stabilize isolated charges. Reducing positive contribution of ion self-diffusion (Figure S5) along with the decreasing negative contribution of ion pairing results in a conductivity maximum at ∼3 GPa along the 1073 K isotherm, as shown in Figure 2b.

In the case of the ReaxFF model, there is a significantly higher negative contribution of the cross-correlation of oppositely charged ions along all three studied isotherms, as shown in Figure 3 (left). In contrast to the SPC/E model, σ in the ReaxFF model is governed by both ion self-diffusion and

https://doi.org/10.1021/acsearthspacechem.5c00139
ACS Earth Space Chem. 2025, 9, 2313−2323

Table 3. Percentage of Free Ions in 1.05 Mol/Kg Solution at Different Conditions from the SPC/E and ReaxFF Models[ab]

Temperature	Pressure	SPC/E (Cl^-, Na^+)	ReaxFF (Cl, Na)
473 K	1.0 GPa	78, 67	35, 34
	2.0 GPa	79, 68	54, 53
	3.0 GPa	79, 70	66, 66
	4.0 GPa	80, 72	77, 77
	5.0 GPa	80, 73	80, 79
673 K	1.0 GPa	65, 62	17, 22
	2.0 GPa	69, 65	29, 34
	3.0 GPa	71, 65	37, 41
	4.0 GPa	71, 66	45, 48
	5.0 GPa	72, 66	53, 55
1073 K	1.0 GPa	43, 42	24, 25
	2.0 GPa	53, 51	26, 30
	3.0 GPa	56, 54	28, 34
	4.0 GPa	59, 55	31, 37
	5.0 GPa	60, 56	34, 40

[a]Convergence plots are shown in Figures S6 and S7. [b]Values are determined by identifying Na and Cl bearing clusters with inter-ionic distances <4.2 Å using a topological approach implemented in the TRAVIS code.[54]

ion pairing, particularly at low pressures. The negative contribution decreases with pressure along all three isotherms due to the reasons discussed above. This is corroborated by the data in Table 3 that show increasing percentages of free cations and anions with pressure along all three isotherms for the ReaxFF model. The total positive contribution from ion self-diffusion also decreases with increasing pressure (Figure S5). The interplay of these two factors results in a non-monotonic behavior of conductivity in the ReaxFF model along all studied isotherms, as shown in Figure 2a. The absolute changes in σ from ReaxFF are rather small in the entire range of P and T considered here, i.e., their values all lie between 10 and 20 S/m.

Note that the contribution of ion self-diffusion to σ is not only a function of D_I of the ions, but also of the ionic charges and density of the system (eq 4). Hence, higher D_I of ions in the ReaxFF model does not necessarily translate to a higher contribution to σ (Figure S5). The higher D_I is offset by lower densities and lower charges predicted by the ReaxFF model. Na^+ and Cl^- ions are treated as hard spheres with fixed formal charges of +1 and −1 respectively in SPC/E model. The ReaxFF model, on the other hand is based on the electronegativity equalization principle[55] that allows for long-range charge transfers leading to partial charges on the ions. Average charges on the ions obtained from the ReaxFF simulations are shown in Table S7.

To check whether partial charges affect the ReaxFF model results, we recalculated σ with formal charges in eq 4. Blazquez et al.[39] argued similarly that although empirical force fields with partial charges give a better estimation of self-diffusion coefficients, formal charges are required to reproduce absolute values of σ at room temperature and pressure. We find that the use of formal charges results in a maximum increase of ∼13 S/

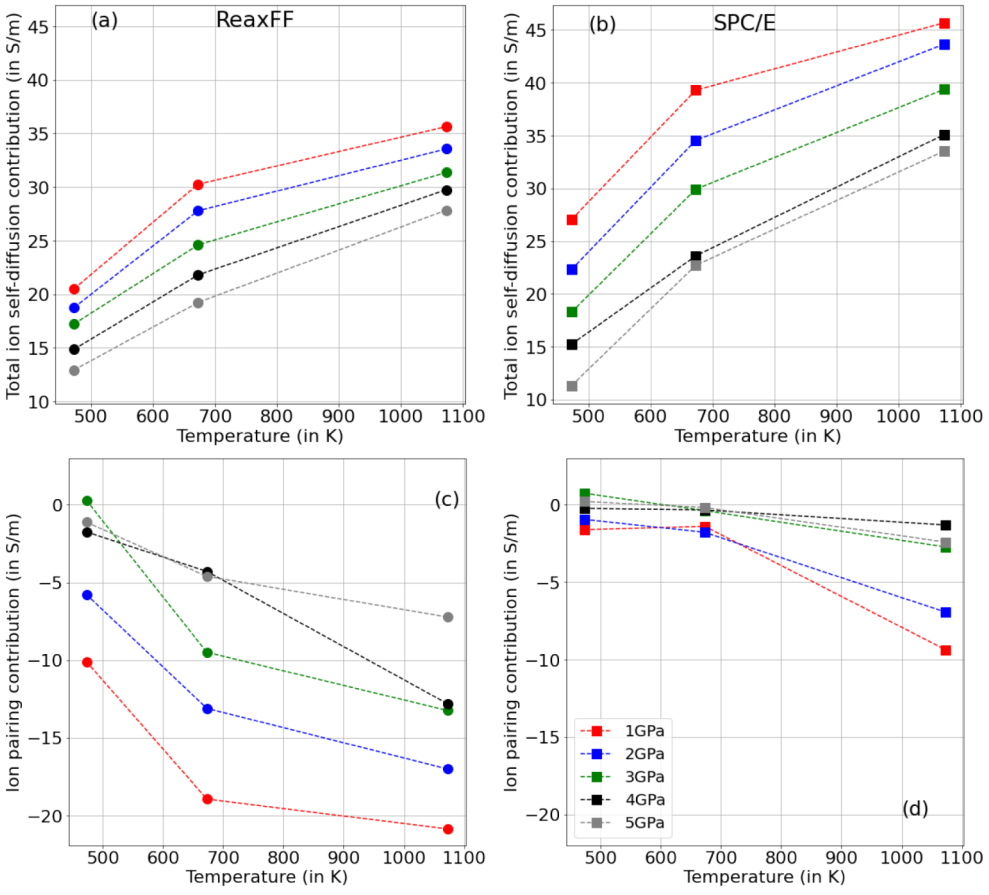

Figure 4. Contribution of ion diffusion and ion pairing to σ in the ReaxFF (a, c) and SPC/E (b, d) along different isobars in 1.05 mol/kg solutions.

https://doi.org/10.1021/acsearthspacechem.5c00139
ACS Earth Space Chem. 2025, 9, 2313−2323

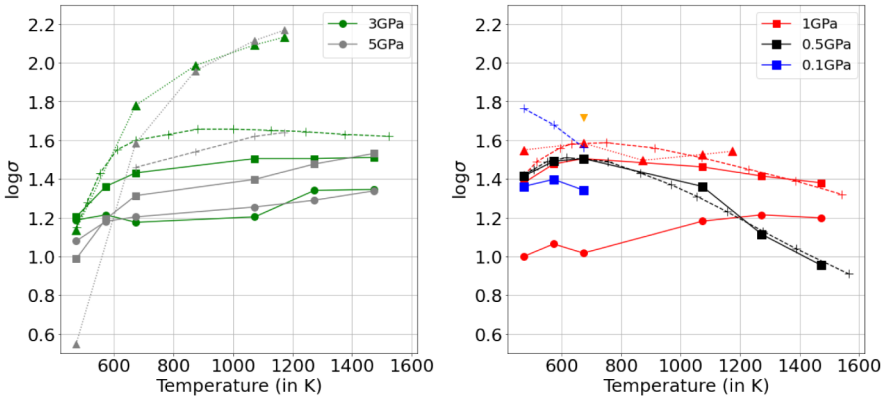

Figure 5. Left: Comparison of σ from the ReaxFF model (dot), SPC/E model (square) and experimental data of Sinmyo and Keppler[21] (plus), Guo and Keppler (triangle)[25] at 3 and 5 GPa. Right: Comparison of σ from the ReaxFF model (dot), SPC/E model (square) with the experimental data from Sinmyo and Keppler[21] (plus), Guo and Keppler[25] (triangle) at 1 GPa, 0.5 and 0.1 GPa. Low salinity data from Reynard et al.[6] is extrapolated to simulation conditions and shown with orange inverted triangle. Data from Sinmyo and Keppler[21] at 3 and 5 GPa pressures are obtained by extrapolating experimental data up to 1 GPa using the equation described in their paper. Different line styles used for simulation and experimental data (solid: MD simulation data, dashed: experimental data from Sinmyo and Keppler[21] and its extrapolations, dotted: experimental data from Guo and Keppler[25]) are guides to the eye. Numerical data for σ along 0.1 and 0.5 GPa isobars with the SPC/E model is listed in Table S9.

m in σ thereby improving the agreement between the two models, as shown in Figure S8.

Since ReaxFF is a dissociative force field, formation of charged species like OH^-, H_3O^+ and $H_5O_2^+$ can also affect σ. Visual inspection of the simulation trajectories confirm the presence of some charged species at 3 of the studied conditions −1 GPa, 2 and 5 GPa at 1073 K. To get an estimate of the contributions of these species to σ, simulations are performed at these conditions and electrical conductivity of the full simulation box containing all the charged species is calculated. Comparison of σ of only Na and Cl ions and the full simulation cell including all the charged species indicates a maximum difference of up to ∼0.2 log units due to the charged species (Figure S9). This result is not surprising because simulation trajectories confirm that these species are transient with lifetimes of few hundred femtoseconds.

Overall, larger ϵ predicted by the SPC/E model (Figure 1 (right)) results in higher percentages of free ions compared to the ReaxFF model along the three isotherms, as shown in Table 3. As a result, σ from the SPC/E model is primarily diffusion driven at lower temperatures. In the case of the ReaxFF model, the ion association is higher and σ is governed by diffusion as well as ion association along all isotherms.

4.1.2. Temperature Dependence. One of the important kinetic models used to explain the temperature dependence of σ of liquids is the Arrhenius law,

$$\sigma = \sigma_0 e^{-\frac{\Delta H}{k_B T}} \quad (9)$$

where σ_0 is the pre-exponential factor and ΔH is the activation enthalpy of the conduction process. For a pure kinetically driven conduction mechanism, the conductivity would increase with temperature. This is the case for the contribution from ion self-diffusion as shown in Figure 4(a,b). This is accompanied by an increase in the negative contribution of ion pairing with increasing temperature at all pressures due to the decreasing ϵ of water, as shown in Figure 4(c,d). Both the models show an increase in σ up to ∼673 K due to the dominance of ion self-diffusion. At higher temperatures, a reversal of the temperature dependence of σ is seen along the 1 and 2 GPa isobars for the SPC/E model due to the competing effects of ion self-diffusion and ion pairing. These effects also result in a non-monotonic temperature dependence of σ obtained from the ReaxFF model.

4.2. Comparison to Experimental Data. Figure 5 compares variations in σ obtained from the SPC/E and ReaxFF models with experimental data sets of Guo and Keppler[25] and Sinmyo and Keppler.[21] Good agreement is observed in the absolute values of σ obtained from the SPC/E model and experimental data and its extrapolations by Sinmyo and Keppler[21] from 0.1 to 5 GPa and by Guo and Keppler[25] at 1 GPa (maximum difference of 0.1 to 0.3 log units). The absolute values of σ obtained from the ReaxFF model differ up to 0.6 log units from the same experimental data. It is interesting to note that the SPC/E model reproduces the experimentally predicted change in temperature dependence from low to high pressures (Figure 5). It predicts increasing conductivity with temperature up to about 400 °C. At higher temperatures, the behavior is pressure dependent. At lower pressures (<1 GPa), σ decreases with increasing temperature (Figure 5 (right), whereas it increases with temperature at higher pressures (>3 GPa) similar to extrapolations of the experimental data of Sinmyo and Keppler[21] (Figure 5 (left).

The distinct change in the temperature dependence observed in the SPC/E simulations motivates the decomposition of the studied temperature and pressure ranges into two distinct regimes depending on the main factor controlling σ—the regime dominated by ion self-diffusion and the regime dominated by ion association, as shown in Figure S10. Since the data from SPC/E shows a roughly linear decrease with pressure at 473 and 673 K, we linearly extrapolated these isotherms to lower pressure and compared them to the data from Bannard,[18] as shown in Figure S11. Their data predict an almost constant conductivity along isotherms up to 0.2 GPa. Extrapolations of the data obtained from the SPC/E simulations to such low pressures show good agreement (within ∼0.3 log units) with this data set. Agreement within <∼0.1 log units is also noted when simulation data is compared against the extrapolation of low-salinity conductivity data from Reynard et al.[6] as shown in Figure 5 (right).

https://doi.org/10.1021/acsearthspacechem.5c00139
ACS Earth Space Chem. 2025, 9, 2313−2323

Larger differences (~0.6−0.8 log units for the SPC/E model and >~1 log units for the ReaxFF model) are observed when absolute values of σ obtained from MD simulations are compared with 3−5 GPa data from Guo and Keppler,[25] particularly at high temperatures. However, as shown in Figure 5 (left), differences of similar magnitudes are also observed in this pressure range between the measured data by Guo and Keppler[25] and the extrapolated data by Sinmyo and Keppler.[21] While both the MD models predict a saturation of σ along the 3 to 5 GPa isobars, experimental data of Guo and Keppler[25] exhibit a strong positive T-dependence. Both experimental studies used different assumptions and extrapolations of theoretical models in treating their high-temperature and high-pressure experimental data, but the reason for these large differences remains unclear. As the Guo and Keppler data is the only experimental high-pressure data set above 1 GPa, there is clearly need for additional measurements.

Interestingly, electrical conductivity measurements of aqueous KCl solutions by Vlasov and Keppler[26] did not show this divergence along the 3 to 5 GPa isobars. To verify this behavior, we performed additional MD simulations of 1 mol/kg aqueous KCl solutions at various temperatures and pressures of 3 and 5 GPa. Our data, shown in Figure S15, reproduces a plateau at high temperatures as obtained in the experimental measurements by Vlasov and Keppler[26] (although there is a quantitative discrepancy of ~0.5 log units). The authors have argued that the difference in the temperature dependence of σ between aqueous NaCl and KCl solutions is due to the collapse of ion hydration shells at high P/T conditions, which makes NaCl more mobile due to its lower mass. However, we do not observe such a hydration shell collapse at any of the studied P/T conditions (Figures S12 and S14). Experimental data from Yamaguchi et al.[56] up to 1.7 GPa and *ab initio* MD data from Rozsa and Galli[57] for Li^+, K^+ and Cl^- ions up to 11 GPa also show the presence of structured hydration shells. Consequently, either the simulations fail to capture an important conduction mechanism that is more relevant for NaCl than for KCl solutions or the electrical conductivities at 3 and 5 GPa presented by Guo and Keppler are too high (or both).

A possible reason for the observed differences between the predictions from MD simulations and the high-pressure experimental data from the simulation side could be the shortcomings of the interaction potentials. This includes the potential functions themselves and they way they were parametrized. In particular, the SPC/E potential is based on a simplified ionic model for the ions with formal charges. It is non-dissociative, i.e., Na^+ and Cl^- are the only possible charged basis species necessary for ionic transport. In addition, none of the force fields used in this study is optimized to reproduce the transport properties at high P/T conditions. The SPC/E potential is parametrized by reference to the experimental heat of vaporization.[46] The ion−water interaction parameters are fitted to gas-phase binding enthalpy data of ion−water clusters.[58] On the contrary, ReaxFF is fitted to quantum chemical data like H−H, HO−OH and O=O bond dissociation energies, charge distributions, angle bending energies, binding energies of water clusters, gas-phase energies of ion−water clusters and EOS of different crystalline phases.[45,59] It includes NaCl potential energy surface scans but these are constrained geometry-optimized gas phase clusters[45] which lack the thermal disorder and long-ranged correlations observed in our simulations. Despite their different functional forms, both potentials qualitatively predict the same behavior of σ at high P/T conditions. Therefore, a dedicated reoptimization of the potential parameters at supercritical conditions is expected to result only in a moderate change in absolute values of σ, but the very high conductivities observed by Guo and Keppler would still be unexplained.

4.3. Geological Implications. Geophysical investigations have revealed the presence of regions characterized by anomalously high electrical conductivities.[60,61] This is often observed in shallow depth subduction zone settings where the predicted temperatures are too low for melting. Guo and Keppler used their experimental data along with the Hashin and Shtrikman[62] upper bound (HS+) model to estimate volume fractions of aqueous fluids containing ~5 wt % NaCl that are required to reproduce geophysical measurements of bulk conductivities in different zones of anomaly. The HS+ model is given by

$$\sigma_{\text{bulk}} = \sigma_e + \frac{1-\phi}{\frac{1}{\sigma_s-\sigma_e} + \frac{\phi}{3\sigma_e}} \tag{10}$$

where σ_{bulk} is the bulk conductivity of the fluid-rock system, σ_e is the conductivity of the NaCl solution, σ_s is the conductivity of the solid matrix, which is taken as 0.001 S/m,[31] and ϕ is the porosity. Since the data from the SPC/E model shows good agreement with the experimental data (and extrapolations) from Sinmyo and Keppler,[21] we use the HS+ model along with the conductivity data from our SPC/E simulations to understand the differences in fluid fraction predictions obtained using our simulation results and the experimental data sets of Guo and Keppler[25] and Sinmyo and Keppler.[21] The data used for fluid fraction calculations using eq 10 is listed in Table S8.

In general, calculated values of fluid fractions from our data are within the range of experimental data of Guo and Keppler[25] at pressures below 1 GPa. For example, SPC/E simulations predict fluid fractions of 0.4−0.6% vs 0.3−1.2% from the experiments of Guo and Keppler[25] (see their Figure S9) in the anomalous region in Casadia (British Columbia)[3] ($T \sim 1173$ K, $P \sim 0.5$−1 GPa). However, big differences in fluid fractions are predicted in the regions of high temperature and high pressure. For example, MD simulations and extrapolated data from Sinmyo and Keppler[21] lead to 0.1−0.3% fluid fraction vs ~0.04% from the Guo and Keppler[25] data set (their Figure S9) in the anomalous zone in Central Argentina[63] ($T \sim 1023$ K, $P \sim 2$−5 GPa). This result is a direct consequence of the lower σ predicted by MD simulations at high temperature and high pressure conditions compared to the Guo and Keppler[25] data set (Figure 5).

All of these values should be taken qualitatively due to the underlying assumptions of the HS+ model and the different assumptions made in the models used to treat the experimental data.[21,25] Note also that we have completely ignored the presence of partial melts in this analysis, which is important in some volcanic arc settings where temperatures are high enough for the formation of partial melts.[60] The presence of small volumes (~1%) of aqueous fluids can explain the anomalously high conductivity in regions such as the deep crust below Tibet.[64] However, fluids cannot explain the reduction in seismic velocities induced by partial melting observed in these regions.[65] Therefore, an interesting extension of this study could be to calculate the electrical conductivity of partial melts

https://doi.org/10.1021/acsearthspacechem.5c00139
ACS Earth Space Chem. 2025, 9, 2313−2323

with MD simulations and then develop a more comprehensive model with the simulation results.

5. CONCLUSIONS

In this paper, we have calculated the electrical conductivity of 1.05 mol/kg NaCl solutions from MD simulations using the ReaxFF and SPC/E interaction potentials over a wide density range of 0.5−1.5 g/cm^3 and temperatures from 473 to 1073 K. Our simulations establish ion self-diffusion and ion association as the two main factors governing σ with the later being responsible for the observed non-monotonic behavior of σ at supercritical conditions. However, the influence of these factors on σ is different for the two models. For the SPC/E model, conductivity is entirely diffusion-driven at lower temperatures, and dominant ion association effects are observed at high temperatures. On the contrary, σ from the ReaxFF model is governed by both the self-diffusion of the ion and the association of the ion at all temperatures and pressures studied. The ReaxFF model predicts the lowest bulk densities and electrical conductivities of all experimental and simulation data considered here. This is related to a higher association of NaCl under supercritical solutions compared to that of the SPC/E model. The simulation results are rather consistent with the partially extrapolated experimental data by Sinmyo and Keppler,[21] whereas large differences are observed with respect to the only data set measured up to 5 GPa by Guo and Keppler.[25]

Considering the limited experimental data, it is difficult to decide whether the simulation models used in this study capture the essential contributions to a reliable prediction of the electrical conductivity of NaCl solutions at high pressures and high temperatures. Further constraints on this important property, especially at high temperatures and pressures above 1 GPa, will be required to improve the interpretation of geophysical conductivity measurements in terms of the fraction and connectivity of fluids in crustal and upper mantle structures.

■ ASSOCIATED CONTENT

Supporting Information

The Supporting Information is available free of charge at https://pubs.acs.org/doi/10.1021/acsearthspacechem.5c00139.

Numerical values of the calculated physical properties, convergence plots, and other related information (PDF)

■ AUTHOR INFORMATION

Corresponding Author

Rajorshi Chattopadhyay − *Institute of Geology and Mineralogy, University of Cologne, Köln 50674, Germany; Department of Earth and Environmental Sciences, Ludwig-Maximilians University Munich, München 80333, Germany;* orcid.org/0009-0008-3812-3731; Email: R.Chattopadhyay@lmu.de

Author

Sandro Jahn − *Institute of Geology and Mineralogy, University of Cologne, Köln 50674, Germany; Department of Earth and Environmental Sciences, Ludwig-Maximilians University Munich, München 80333, Germany;* orcid.org/0000-0002-2137-8833

Complete contact information is available at: https://pubs.acs.org/10.1021/acsearthspacechem.5c00139

Notes

The authors declare no competing financial interest.

■ ACKNOWLEDGMENTS

This study was supported by the Deutsche Forschungsgemeinschaft (DFG) in the framework of project JA 1469/13-1. The authors gratefully acknowledge the Gauss Centre for Supercomputing e.V. (www.gauss-centre.eu) for funding this project by providing computing time through the John von Neumann Institute for Computing (NIC) on the GCS Supercomputer JUWELS at Jülich Supercomputing Centre (JSC). The authors would also like to thank the editor and the reviewers whose constructive reviews significantly improved the overall quality of the research paper.

■ REFERENCES

(1) Ichihara, H.; Sakanaka, S.; Mishina, M.; Uyeshima, M.; Nishitani, T.; Ogawa, Y.; Yamaya, Y.; Mogi, T.; Amita, K.; Miura, T. A 3-D electrical resistivity model beneath the focal zone of the 2008 Iwate-Miyagi Nairiku earthquake (M 7.2). *Earth, Planets Space* **2014**, *66*, 50.

(2) Ichiki, M.; Baba, K.; Toh, H.; Fuji-Ta, K. An overview of electrical conductivity structures of the crust and upper mantle beneath the northwestern Pacific, the Japanese Islands, and continental East Asia. *Gondwana Res* **2009**, *16*, 545−562.

(3) Soyer, W.; Unsworth, M. Deep electrical structure of the northern Cascadia (British Columbia, Canada) subduction zone: Implications for the distribution of fluids. *Geology* **2006**, *34*, 53−56.

(4) Glover, P. W. J.; Ádám, A.Correlation between crustal high conductivity zones and seismic activity and the role of carbon during shear deformation*J. Geophys. Res.: Solid Earth***2008***113*

(5) Guo, X.; Yoshino, T.; Shimojuku, A. Electrical conductivity of albite-(quartz)-water and albite-water-NaCl systems and its implication to the high conductivity anomalies in the continental crust. *Earth Planet. Sci. Lett* **2015**, *412*, 1−9.

(6) Reynard, B.; Mibe, K.; de Moortéle, B. V. Electrical conductivity of the serpentinised mantle and fluid flow in subduction zones. *Earth Planet. Sci. Lett* **2011**, *307*, 387−394.

(7) Hermance, J. F. The electrical conductivity of materials containing partial melt: A simple model from Archie's law. *Geophys. Res. Lett* **1979**, *6*, 613−616.

(8) Roberts, J. J.; Tyburczy, J. A. Partial-melt electrical conductivity: Influence of melt composition. *J. Geophys. Res.: Solid Earth* **1999**, *104*, 7055−7065.

(9) Hyndman, R.; Hyndman, D. Water saturation and high electrical conductivity in the lower continental crust. *Earth Planet. Sci. Lett* **1968**, *4*, 427−432.

(10) Hyndman, R. D.; Shearer, P. M. Water in the lower continental crust: modelling magnetotelluric and seismic reflection results*. *Geophys. J. Int* **1989**, *98*, 343−365.

(11) Shimojuku, A.; Yoshino, T.; Yamazaki, D.; Okudaira, T. Electrical conductivity of fluid-bearing quartzite under lower crustal conditions. *Phys. Earth Planet. Inter* **2012**, *198−199*, 1−8.

(12) Shimojuku, A.; Yoshino, T.; Yamazaki, D. Electrical conductivity of brine-bearing quartzite at 1 GPa: implications for fluid content and salinity of the crust. *Earth, Planets Space* **2014**, *66*, 2.

(13) Quist, A. S. Ionization constant of water to 800° and 4000 bar. *J. Phys. Chem* **1970**, *74*, 3396−3402.

(14) Marshall, W. L.; Franck, E. U. Ion product of water substance, 0−1000°C, 1−10,000 bar New International Formulation and its background. *J. Phys. Chem. Ref. Data* **1981**, *10*, 295−304.

(15) Kawamoto, T.; Yoshikawa, M.; Kumagai, Y.; Mirabueno, M. H. T.; Okuno, M.; Kobayashi, T. Mantle wedge infiltrated with saline fluids from dehydration and decarbonation of subducting slab. *Proc. Int. Acad. Sci* **2013**, *110*, 9663−9668.

(16) Chen, L.; Booker, J. R.; Jones, A. G.; Wu, N.; Unsworth, M. J.; Wei, W.; Tan, H. Electrically Conductive Crust in Southern Tibet from INDEPTH Magnetotelluric Surveying. *Science* **1996**, *274*, 1694−1696.
(17) Le Pape, F.; Jones, A.; Vozar, J.; Wenbo, W. Penetration of crustal melt beyond the Kunlun Fault into Northern Tibet. *Nat. Geosci* **2012**, *5*, 330−335.
(18) Bannard, J. E. Effect of density on the electrical conductance of aqueous sodium chloride solutions. *J. Appl. Electrochem* **1975**, *5*, 43−53.
(19) Quist, A. S.; Marshall, W. L. Electrical conductances of aqueous sodium chloride solutions from 0 to 800°C and at pressures to 4000 bar. *J. Phys. Chem* **1968**, *72*, 684−703.
(20) Ho, P. C.; Palmer, D. A.; Mesmer, R. E. Electrical conductivity measurements of aqueous sodium chloride solutions to 600°C and 300 MPa. *J. Solution Chem* **1994**, *23*, 997−1018.
(21) Sinmyo, R.; Keppler, H. Electrical conductivity of NaCl-bearing aqueous fluids to 600 °C and 1 GPa. *Contrib. Mineral. Petrol* **2017**, *172*, 4.
(22) Fogo, J. K.; Benson, S. W.; Copeland, C. S. The Electrical Conductivity of Supercritical Solutions of Sodium Chloride and Water. *J. Chem. Phys* **1954**, *22*, 212−216.
(23) Corwin, J. F.; Bayless, R. G.; Owen, G. E. The conductivity of dilute sodium chloride solutions under supercritical conditions[1]. *J. Phys. Chem* **1960**, *64*, 641−646.
(24) Lee, S.; Cummings, P.; Simonson, J.; Mesmer, R. Molecular dynamics simulation of the limiting conductance of NaCl in supercritical water. *Chem. Phys. Lett* **1998**, *293*, 289−294.
(25) Guo, H.; Keppler, H. Electrical Conductivity of NaCl-Bearing Aqueous Fluids to 900°C and 5 GPa. *J. Geophys. Res.: Solid Earth* **2019**, *124*, 1397−1411.
(26) Vlasov, K.; Keppler, H. Electrical Conductivity of KCl-H2O Fluids in the Crust and Lithospheric Mantle. *J. Geophys. Res.: Solid Earth* **2022**, *127*, No. e2022JB024080.
(27) Ghaffari, A.; Rahbar-Kelishami, A. MD simulation and evaluation of the self-diffusion coefficients in aqueous NaCl solutions at different temperatures and concentrations. *J. Mol. Liq* **2013**, *187*, 238−245.
(28) Chakraborty, D.; Chandra, A. Diffusion of ions in supercritical water: Dependence on ion size and solvent density and roles of voids and necks. *J. Mol. Liq* **2011**, *162*, 12−19.
(29) Mallik, B. S.; Chandra, A. Hydrogen bond and residence dynamics of ion−water and water−water pairs in supercritical aqueous ionic solutions: Dependence on ion size and density. *J. Chem. Phys* **2006**, *125*, 234502.
(30) Sherman, D. M.; Collings, M. D. Ion association in concentrated NaCl brines from ambient to supercritical conditions: Results from classical molecular dynamics simulations. *Geochem. Trans* **2002**, *3*, 102−107.
(31) Sakuma, H.; Ichiki, M. Electrical conductivity of NaCl-H_2O fluid in the crust. *J. Geophys. Res.: Solid Earth* **2016**, *121*, 577−594.
(32) Yoon, T. J.; Patel, L. A.; Vigil, M. J.; Maerzke, K. A.; Findikoglu, A. T.; Currier, R. P. Electrical conductivity, ion pairing, and ion self-diffusion in aqueous NaCl solutions at elevated temperatures and pressures. *J. Chem. Phys* **2019**, *151* (22), 224504.
(33) Lyubartsev, A. P.; Laaksonen, A. Concentration Effects in Aqueous NaCl Solutions. A Molecular Dynamics Simulation. *J. Phys. Chem* **1996**, *100*, 16410−16418.
(34) Pan, Y.; Yong, W.; Secco, R. A. Electrical Conductivity of Aqueous NaCl at High Pressure and Low Temperature: Application to Deep Subsurface Oceans of Icy Moons. *Geophys. Res. Lett* **2021**, *48*, No. e2021GL094020.
(35) Sala, J.; Guárdia, E.; Martí, J. Effects of concentration on structure, dielectric, and dynamic properties of aqueous NaCl solutions using a polarizable model. *J. Chem. Phys* **2010**, *132* (21), 214505.
(36) Chowdhuri, S.; Chandra, A. Hydration structure and diffusion of ions in supercooled water: Ion size effects. *J. Chem. Phys* **2003**, *118*, 9719−9725.
(37) Chowdhuri, S.; Chandra, A. Molecular dynamics simulations of aqueous NaCl and KCl solutions: Effects of ion concentration on the single-particle, pair, and collective dynamical properties of ions and water molecules. *J. Chem. Phys* **2001**, *115*, 3732−3741.
(38) Zielkiewicz, J. Structural properties of water: Comparison of the SPC, SPCE, TIP4P, and TIP5P models of water. *J. Chem. Phys* **2005**, *123* (10), 104501.
(39) Blazquez, S.; Abascal, J. L. F.; Lagerweij, J.; Habibi, P.; Dey, P.; Vlugt, T. J. H.; Moultos, O. A.; Vega, C. Computation of Electrical Conductivities of Aqueous Electrolyte Solutions: Two Surfaces, One Property. *J. Chem. Theory Comput* **2023**, *19*, 5380−5393.
(40) Agmon, N. The Grotthuss mechanism. *Chem. Phys. Lett* **1995**, *244*, 456−462.
(41) van Duin, A. C. T.; Dasgupta, S.; Lorant, F.; Goddard, W. A. ReaxFF: A Reactive Force Field for Hydrocarbons. *J. Phys. Chem. A* **2001**, *105*, 9396−9409.
(42) Zhang, W.; van Duin, A. C. T. Improvement of the ReaxFF Description for Functionalized Hydrocarbon/Water Weak Interactions in the Condensed Phase. *J. Phys. Chem. B* **2018**, *122*, 4083−4092.
(43) Shin, Y. K.; Kwak, H.; Vasenkov, A. V.; Sengupta, D.; van Duin, A. C. Development of a ReaxFF Reactive Force Field for Fe/Cr/O/S and Application to Oxidation of Butane over a Pyrite-Covered Cr_2O_3 Catalyst. *ACS Catal* **2015**, *5*, 7226−7236.
(44) Manzano, H.; Zhang, W.; Raju, M.; Dolado, J. S.; López-Arbeloa, I.; van Duin, A. C. T. Benchmark of ReaxFF force field for subcritical and supercritical water. *J. Chem. Phys* **2018**, *148*, 234503.
(45) Fedkin, M. V.; Shin, Y. K.; Dasgupta, N.; Yeon, J.; Zhang, W.; van Duin, D.; van Duin, A. C. T.; Mori, K.; Fujiwara, A.; Machida, M.; Nakamura, H.; Okumura, M. Development of the ReaxFF Methodology for Electrolyte-Water Systems. *J. Phys. Chem. A* **2019**, *123*, 2125−2141.
(46) Berendsen, H. J. C.; Grigera, J. R.; Straatsma, T. P. The missing term in effective pair potentials. *J. Phys. Chem* **1987**, *91*, 6269−6271.
(47) Thompson, A. P.; Aktulga, H. M.; Berger, R.; Bolintineanu, D. S.; Brown, W. M.; Crozier, P. S.; in'tVeld, P. J.; Kohlmeyer, A.; Moore, S. G.; Nguyen, T. D.; Shan, R.; Stevens, M. J.; Tranchida, J.; Trott, C.; Plimpton, S. J. LAMMPS - a flexible simulation tool for particle-based materials modeling at the atomic, meso, and continuum scales. *Comput. Phys. Commun* **2022**, *271*, 108171.
(48) Green, M. S. Markoff Random Processes and the Statistical Mechanics of Time-Dependent Phenomena. II. Irreversible Processes in Fluids. *J. Chem. Phys* **1954**, *22*, 398−413.
(49) Kubo, R. Statistical-Mechanical Theory of Irreversible Processes. I. General Theory and Simple Applications to Magnetic and Conduction Problems. *J. Phys. Soc. Jpn* **1957**, *12*, 570−586.
(50) Tu, K.-M.; Ishizuka, R.; Matubayasi, N. Spatial-decomposition analysis of electrical conductivity in concentrated electrolyte solution. *J. Chem. Phys* **2014**, *141* (4), 044126.
(51) Yeh, I.-C.; Hummer, G. System-Size Dependence of Diffusion Coefficients and Viscosities from Molecular Dynamics Simulations with Periodic Boundary Conditions. *J. Phys. Chem. B* **2004**, *108*, 15873−15879.
(52) Mantegazzi, D.; Sanchez-Valle, C.; Driesner, T. Thermodynamic properties of aqueous NaCl solutions to 1073K and 4.5 GPa, and implications for dehydration reactions in subducting slabs. *Geochim. Cosmochim. Acta* **2013**, *121*, 263−290.
(53) Sverjensky, D. A.; Harrison, B.; Azzolini, D. Water in the deep Earth: The dielectric constant and the solubilities of quartz and corundum to 60kb and 1200°C. *Geochim. Cosmochim. Acta* **2014**, *129*, 125−145.
(54) Brehm, M.; Thomas, M.; Gehrke, S.; Kirchner, B. TRAVIS—A free analyzer for trajectories from molecular simulation. *J. Chem. Phys* **2020**, *152*, 164105.
(55) Mortier, W. J.; Ghosh, S. K.; Shankar, S. Electronegativity-equalization method for the calculation of atomic charges in molecules. *J. Am. Chem. Soc* **1986**, *108*, 4315−4320.
(56) Yamaguchi, T.; Fukuyama, N.; Yoshida, K.; Katayama, Y. Ion Solvation and Water Structure in an Aqueous Sodium Chloride

Solution in the Gigapascal Pressure Range. *J. Phys. Chem. Lett* **2021**, *12*, 250−256.
(57) Rozsa, V.; Galli, G. Solvation of simple ions in water at extreme conditions. *J. Chem. Phys* **2021**, *154* (14), 144501.
(58) Smith, D. E.; Dang, L. X. Computer simulations of NaCl association in polarizable water. *J. Chem. Phys* **1994**, *100*, 3757−3766.
(59) van Duin, A. C. T.; Zou, C.; Joshi, K.; Bryantsev, V.; Goddard, W. A. A ReaxFF Reactive Force-field for Proton Transfer Reactions in Bulk Water and its Applications to Heterogeneous Catalysis. In *Computational Catalysis* Royal Society of Chemistry: 2024.
(60) Syracuse, E. M.; van Keken, P. E.; Abers, G. A. The global range of subduction zone thermal models. *Phys. Earth Planet. Inter* **2010**, *183*, 73−90.
(61) Pommier, A. Geophysical assessment of migration and storage conditions of fluids in subduction zones. *Earth, Planets Space* **2014**, *66*, 38.
(62) Hashin, Z.; Shtrikman, S. A Variational Approach to the Theory of the Effective Magnetic Permeability of Multiphase Materials. *J. Appl. Phys* **1962**, *33*, 3125−3131.
(63) Booker, J. R.; Favetto, A.; Pomposiello, M. C. Low electrical resistivity associated with plunging of the Nazca flat slab beneath Argentina. *Nature* **2004**, *429*, 399−403.
(64) Pham, V. N.; Boyer, D.; Therme, P.; Yuan, X. C.; Li, L.; Jin, G. Y. Partial melting zones in the crust in southern Tibet from magnetotelluric results. *Nature* **1986**, *319*, 310−314.
(65) Gaillard, F.; Scaillet, B.; Pichavant, M. Pichavant Evidence for present-day leucogranite pluton growth in Tibet. *Geology* **2004**, *32*, 801−804.

https://doi.org/10.1021/acsearthspacechem.5c00139
ACS Earth Space Chem. 2025, 9, 2313−2323